EPJ Web of Conferences **183**, 02045 (2018) https://doi.org/10.1051/epjconf/201818302045
DYMAT 2018

Testing of Auxetic Materials Using Hopkinson Bar and Digital Image Correlation

Tomáš Fíla[1,*], *Petr* Zlámal[1], *Jan* Falta[1], *Tomáš* Doktor[1], *Petr* Koudelka[1], *Daniel* Kytýř[1], *Marcel* Adorna[1], *Jutta* Luksch[2], *Michaela* Neuhäuserová[1], *Jaroslav* Valach[3], and *Ondřej* Jiroušek[1]

[1]Czech Technical University in Prague, Faculty of Transportation Sciences, Konviktská 20, 110 00 Prague, Czech Republic
[2]Universität des Saarlandes, Institute of Applied Mechanics, Campus A4.2, Saarbrücken, 66123, Germany
[3]Czech Academy of Sciences, Institute of Theoretical and Applied Mechanics, Prosecká 76, 190 00 Prague, Czech Republic

Abstract. In this paper, a split Hopkinson pressure bar (SHPB) was used for impact loading of an auxetic lattice (structure with negative Poisson's ratio) at a given strain-rate. High strength aluminum and polymethyl methacrylate bars instrumented with foil strain-gauges were used for compression of an additively manufactured missing-rib auxetic lattice. All experiments were observed using a high-speed camera with frame-rate set to approx. 135.000 fps. High-speed images were synchronized with the strain-gauge records. Dynamic equilibrium in the specimen was analyzed and optimized pulse-shaping was introduced in the selected experiments. Longitudinal and lateral in-plane displacements and strains were evaluated using digital image correlation (DIC) technique. DIC results were compared with results obtained from strain-gauges and were found to be in good agreement. Using DIC, it was possible to analyze in-plane strain distribution in the specimens and to evaluate strain dependent Poisson's ratio of the auxetic structure.

1 Introduction

Modern manufacturing technologies such as foaming of metals, advanced coating procedures or additive manufacturing allow for development of advanced cellular metals suitable for energy absorption applications [1]. Testing of such materials under dynamic loading is necessary to evaluate their mechanical properties relevant to the proposed application. Additive manufacturing allows for design of highly advanced materials such as auxetic lattices exhibiting negative Poisson's ratio [2, 3]. For such materials, conventional analysis in dynamic crushing is not sufficient and advanced experimental methods have to be employed [4]. In dynamic loading, some studies concentrated on materials with microstructure used digital image correlation (DIC) of high-speed camera images as a tool for full-field analysis of strain and other phenomena in the specimen [4–7]. In this paper, we use SHPB for dynamic compression of an additively manufactured auxetic lattice and DIC is used for an advanced analysis of its deformation behavior.

2 Materials and methods

2.1 Specimen

In the experimental study, the constructs based on the missing-rib unit-cell geometry were subjected to dynamic compression and compared with quasi-static results. Geometry of such a unit-cell is derived from periodical arrangement of squares by removing selected ribs and by rotating the structure by 45 degrees in the direction of loading. The resulting microstructure then exhibits in-plane negative strain-dependent Poisson's ratio. Selective laser sintering (SLS) method was selected for production of the samples and manufacturing was performed using the AM250 system (Renishaw, UK) by sintering the 316L-0407 powdered austenitic steel. The cuboid constructs were designed using a parametric modeler according to constraints given by the dimensions of SHPB setup and requirements for dimension of the representative volume element (RVE) of the structure. Thus, square cross-section with edge length 12.15 mm and height of the samples 12.58 mm were selected in order to minimize inertia and frictional effects in the SHPB experiments. Furthermore, the ratio of approximately one between height of the sample and its cross-sectional dimensions enables to reach the densification region of its response during impact loading. The produced samples (see Fig. 1) were composed of 36 unit cells in 6×6 arrangement at nominal porosity of 74.37 % and thickness of the struts was 0.3 mm, which is close to the limit of the used manufacturing method.

2.2 Experimental setup

Testing of the auxetic structure was performed using a modified Kolsky SHPB setup. Both bars and the striker had the same nominal diameter 20 mm. Two types of materials of the bars and the striker were used in this study to investigate the possibility of using them with this type of structure (material with relatively low mechanical impedance). High-strength aluminium alloy (EN-AW-

*e-mail: fila@fd.cvut.cz

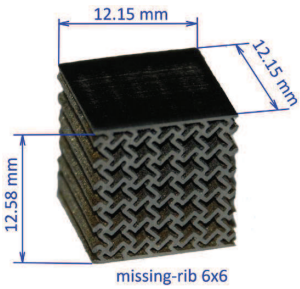

Fig. 1. Tested cubic auxetic lattice - missing-rib, consisting of 6×6 cells, additively manufactured from powdered austenitic steel 316L-0407 using SLS.

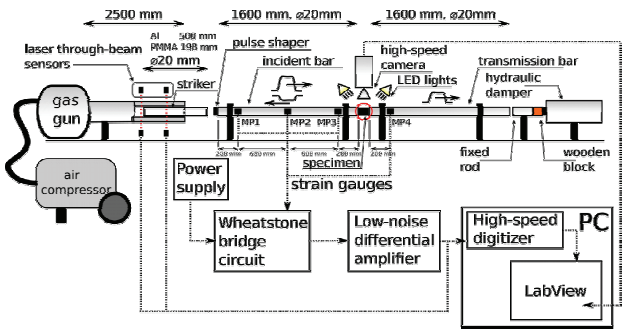

Fig. 2. Scheme of the experimental setup and its function parts.

7075) was selected as a material of the bars with higher mechanical impedance whereas polymethyl methacrylate (PMMA) was chosen as a material with lower mechanical impedance. The striker in a barrel was accelerated using a gas-gun system with 16 bar maximum pressure. The gas-gun system consisted of the steel barrel with the maximal operating length 2500 mm, a high-flow fast release solenoid valve (366531, Parker, USA), a 20 l air reservoir equipped with pressure gauge and other accessories (compressor unit, safety parts, piping etc.). The incident bar and the transmission bar (for both materials - aluminium and PMMA) had the same length 1600 mm and were guided and supported by set of a low-friction polymer-liner slide bearings (Drylin FJUM, IGUS, Germany) with a custom stainless steel housing. The length of the strikers was 500 mm (aluminium) and 198 mm (PMMA). A hydraulic damper and a fixed aluminium rod with a wooden block embedded in between were used to absorb residual kinetic energy of the experiment. Surfaces of the bars were carefully ground and polished to obtain proper diameter tolerance for smooth motion in the bearings. Position of the bar was adjusted in the bearings to minimize friction effects and to achieve suitable straightness of axis of the SHPB setup. Proper geometrical alignment is important in terms of reduction of the undesirable effects (increased friction, bending of the bars etc.) affecting measurement accuracy. The contact faces of the bars were finished using high-precision grinding and polishing and were adjusted to achieve the faces plan-parallelism better than 0.05 mm (measured by feeler gauge). Spurious effects of wave dispersion in the aluminium bars were reduced by pulse-shaping technique. Soft copper pulse-shaper (Cu-ETP R220) with diameter 7 mm and thickness 0.5 mm was used on the basis of results from calibration experiments. This pulse-shaping approach enabled to reach constant strain rates in the plateau region. Dispersion effects in the PMMA bars were corrected using methods described in [8, 9]. Impact velocities of the striker were approx. 21 m/s (aluminium) and approx. 45 m/s (PMMA). Prior to the experiments, all strain gauges ware calibrated using direct force measurement procedure. End of the incident bar was fixed and both bars were gradually loaded using a screw adapter with simultaneous measurement of force using a force transducer (U9b, HBM, Germany). Then, direct force values were compared with the values derived from the strain gauges and proper behaviour of the gauges was verified. Dynamic mechanical properties of both aluminium and PMMA bars were calculated from a calibration void test using aforementioned Bacon's method [8].

2.3 Instrumentation

Four measurement points (MPs) equipped with foil strain gauges in Wheatstone half-bridge arrangement were used for measurement of strain wave during the test. On the incident bar, three MPs were established with geometric alignment: 200 mm (front of bar-MP1), 600 mm (MP1-MP2), 600 mm (MP2-MP3), 200 mm (MP3-end of the bar) whereas on the transmission bar only single MP was set at a distance of 200 mm from the front face of the bar. Foil strain gauges (3/120 LY61, HBM, Germany) were selected because of their linearity and possibility of measurement of higher strain values ($50,000\,\mu\varepsilon$) in comparison with semiconductor gauges ($2,500\,\mu\varepsilon$). On the other hand, the output signal from strain gauges is low and has to be amplified before digitization. To guarantee accurate measurement of the auxetic structures, the strain gauges with 3 mm active gauge length ensuring suitable integration of strain wave were selected. Each strain gauge was bonded on the bar with a single component low-viscosity cyanoacrylate adhesive (Z70, HBM, Germany) and cured for at least 12 hours. Powering of the strain gauge circuits was performed using a custom battery source (with excitation voltage 3.1 V) to decrease measurement noise and maximize signal-to-noise ratio of the output signal. Active differential low noise amplifier (EL-LNA-2, Elsys AG, Switzerland) with gain 100 was used for the amplification of the strain gauge signals before the digitization. The strain gauge signal was sampled using a pair of synchronized high speed 16-bit digitizers (PCI-9826H, ADLINK Technology, Inc., Taiwan) with maximal 20 MHz sample rate. Another two channels of the digitizer were used to acquire a signal from the through-beam photoelectric sensor (FS/FE 10-RL-PS-E4, Sensopart, Germany) installed on the gas-gun barrel at a fixed distance from each other. These signals were used for determination of the striker velocity and for triggering of the digitizers and a high-speed camera as well as for time synchronization of the strain gauge signals with the captured images. The samples were observed using a high-speed camera (FAST-

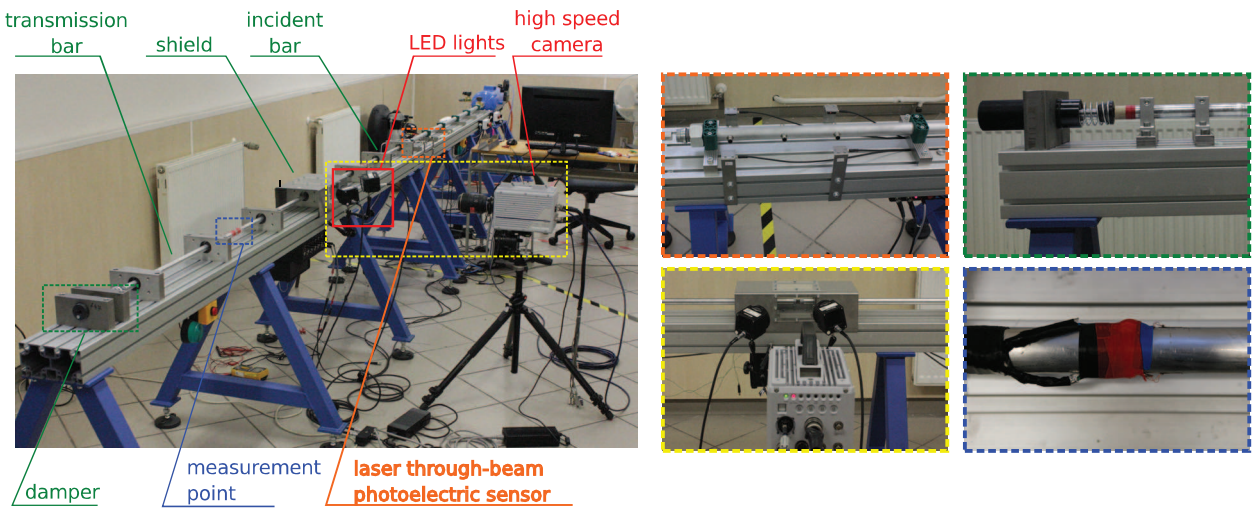

Fig. 3. SHPB experimental setup and detail views showing barrel with photoelectric sensors (orange), hydraulic damper (green), high-speed camera with lighting (yellow) and strain-gauges (blue).

CAM SA5, Photron, Japan) with CMOS sensor having 20 μm pixel size and maximal resolution 1024×1024 pixels. Since the value of maximal frame rate is dependent on the image resolution, region of interest (ROI) was set to 256×168 pixels that enabled to reach frame rate approximately 130 kfps. Selected ROI was scaled to the whole sample area (with sufficient overlap of the ends of both bars) which lead to 5 pixel resolution per strut thickness of the auxetic structure. The scene was illuminated using a pair of high intensity LED lights (Constellation 60, Veritas, USA). Data acquisition and control of instruments of the SHPB setup were employed using a custom virtual instrument designed in Labview environment (National Instruments, USA) and the acquired data were exported to TDMS binary file format for further post-processing and evaluation using custom MATLAB tools.

2.4 Digital Image Correlation

To evaluate in-plane displacement and calculate strain fields in the specimen, DIC technique was used. Basic principle of DIC is based on tracking selected correlation points (pixels) between two images (reference and deformed subset) recorded consecutively during the deformation process. The technique uses a maximisation approach to find the correlation coefficient for the best fit between sub-images defined around the control points set in the reference (undeformed) image. The custom DIC toolkit [10] used in this study works in two steps, where the correlation is initially evaluated at pixel level and, in the second step, Lucas-Kanade algorithm [11] is used to enable sub-pixel accuracy. In the first step (pixel accuracy), the normalized cross-correlation method NCC is used to calculate integer value of the displacement. Deformation mapping function is extracted based on correlation coefficient which is determined by examining pixel intensity of the image subsets according to:

$$r_{ij}(u, v, \frac{\partial u}{\partial x}, \frac{\partial u}{\partial y}, \frac{\partial v}{\partial x}, \frac{\partial v}{\partial y}) = \\ = 1 - \frac{\sum_i \sum_j [I_0(x_i, y_j) - \bar{I}_0][I_1(x_i', y_j') - \bar{I}_1]}{\sqrt{\sum_i \sum_j [I_0(x_i, y_j) - \bar{I}_0]^2 \sum_i \sum_j [I_1(x_i', y_j') - \bar{I}_1]^2}} \quad (1)$$

where $I_0(x_i, y_j)$ is the pixel intensity in the reference image at a point (x_i, y_j) and $I_1(x_i', y_j')$ is the pixel intensity at a point (x_i', y_j') in the deformed image. $\bar{I}_0$ and $\bar{I}_1$ are the mean values of intensity in the images I_0 and I_1, respectively. The maximum of the correlation coefficient is found using steepest-gradient method and a new position of the point is localized where the current sub-image has the best correlation. Second step (sub-pixel accuracy) is performed using Lucas-Kanade tracking algorithm with sub-pixel precision achieved by employing Gauss-Newton nonlinear optimization.

3 Results

3.1 Stress-strain using strain-gauges

In total, seven specimens were tested (4 - aluminium bars, 3 - PMMA bars). Dynamic equilibrium was reached in all experiments with both types of bars (see example plots in Fig. 4). Stress-strain curves were derived from the strain-gauge signals for both types of bars. Corresponding stress-strain curves including standard deviation together with strain-rates and quasi-static data are shown in Fig. 5. SHPB results are in very good agreement and exhibit significant strain-rate effect as the stresses are higher by the factor of approx. 1.4 compared to the quasi-static results. Similar trend was observed in previously published experiments [12]. PMMA bars, in contrary to the aluminium bars, show stress decrease before the densification part.

The effect can be caused by several factors such as strain-rate, difference in friction coefficients and bending stiffness of the bars. Moreover, mechanical impedance of the specimen was on the limit of the used PMMA bars. Due to high impact velocity (45 m/s), extensive non-linear effects, dispersion and damping was observed in the PMMA bars and the effects had to be extensively corrected according to aforementioned methods. However, most probable cause of this distortion can be attributed to slightly different boundary conditions of the experiments as, in case of the PMMA bars, a thin steel washers were placed between the bars' ends and the specimen to prevent damage of the soft surface of the bars. A thin layer of grease was used in the contact. As the missing-rib lattice structure is asymmetric, significant side movement was observed in all experiments (both quasi-static and SHPB). Minor difference between PMMA and aluminium bars can be observed also in other results summarized in the following paragraphs.

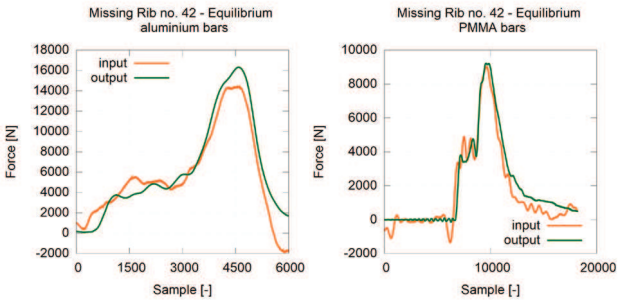

Fig. 4. Examples of measured dynamic equilibrium: aluminium bars (left), PMMA bars (right).

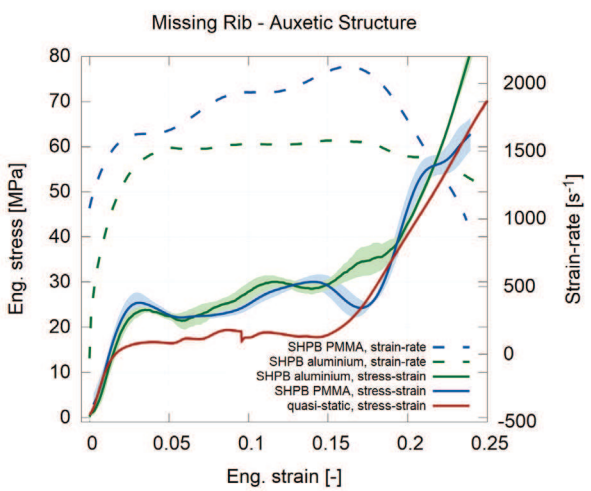

Fig. 5. Stress-strain and strain-rate-strain curves derived from SHPB with aluminium and PMMA bars compared to quasi-static experiments.

3.2 Strain using DIC

Identical grid consisting of 26×17 correlation points covering the area of the sample and the end parts of the measurement bars was placed on the high-speed camera images. The grid was tracked using DIC and new positions of the grid points were identified in every captured image. The high-speed camera images were converted from raw format to 8-bit png by lossless compression algorithm and were not subjected to any additional pre-processing. In all cases, digital image correlation was successful with mean correlation coefficient 95.7 % in the worst case. In every experiment, some of the points lost relevant correlation, particularly the points located on the side edges of the specimen. Based on the image correlation results, four strain values valid for the different parts of the specimen were calculated. Geometric configuration used for the calculation of four different strains is shown in Fig. 6. Following strains were calculated from mean displacement evaluated at the lines shown in Fig. 6:

$$\epsilon_{xx_b} = \frac{u_{11} - u_{12}}{L_{i2}} \tag{2}$$

$$\epsilon_{xx_e} = \frac{u_{21} - u_{22}}{L_{i2}} \tag{3}$$

$$\epsilon_{xx_{in2}} = \frac{u_{31} - u_{32}}{L_{i3}} \tag{4}$$

$$\epsilon_{xx_{in3}} = \frac{u_{41} - u_{42}}{L_{i4}} \tag{5}$$

where u_{jk} corresponds to the longitudinal displacements and L_{in} corresponds to the initial lengths of the relevant part of the specimen. Thus, ϵ_{xx_b} expresses strain calculated using the image correlation data from the random pattern fixed on the measurement bars, ϵ_{xx_e} expresses strain on the edges of the specimens and the other two ($\epsilon_{xx_{in2}}$, $\epsilon_{xx_{in3}}$) are strain values in the specimen's core.

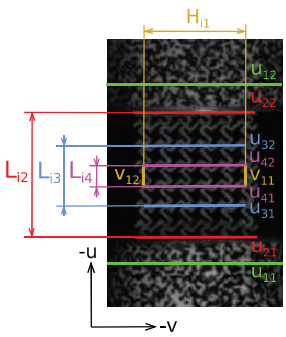

Fig. 6. Geometric configuration of the correlation grid used for strain calculations in a different parts of the specimen.

The strain values calculated using equations (2)-(5) are plotted against the reference strain from the strain-gauge (dashed line) in Fig. 7 and Fig. 8, showing strain development in the different parts of the specimen for both aluminium and PMMA bars. In case of the aluminium bars, strain ϵ_{xx_b} (strain from the bars' ends) is slightly higher than the reference strain and strain ϵ_{xx_e} (strain from the specimen edges) corresponds almost perfectly with the reference strain. This difference corresponds to approximately 2 px of the image and can be considered as the image correlation error. Other possible reasons for this can be attributed to correlation pattern shift during the experiment, optical lenses errors or by minor error in used mechanical parameters of the bars. Strains $\epsilon_{xx_{in2}}$ and $\epsilon_{xx_{in3}}$

show different deformation behavior in the central regions of the specimen as the core deforms with certain time delay than the boundary parts of the specimen. Dotted line expresses strain $\epsilon_{xx_{in3}}$ from the PMMA bars (or the aluminium bars, respectively) showing similar trend, but not the same values. This can be caused by the effects summarized in section 3.1. Strains from the PMMA experiments in Fig. 8 show very good agreement of ϵ_{xx_b} and ϵ_{xx_e}. Moreover, they are in good agreement with the aluminium experiments showing similar deformation behavior.

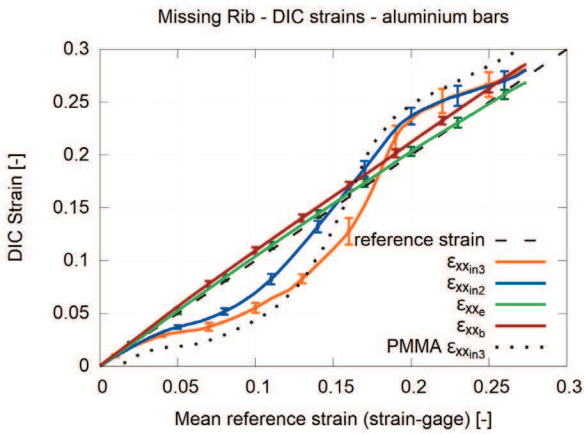

Fig. 7. Comparison of the different DIC strains with the reference strain-gauge signal - aluminium bars.

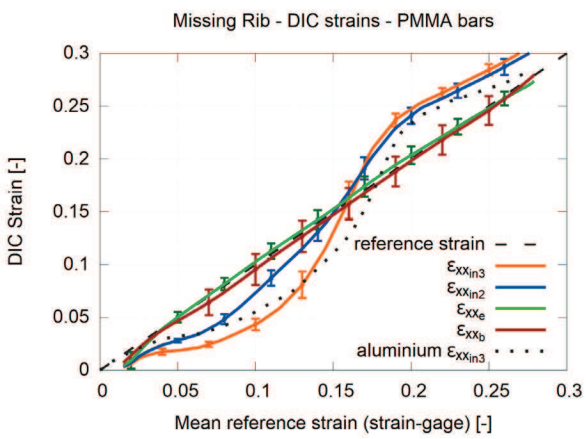

Fig. 8. Comparison of the different DIC strains with the reference strain-gauge signal - PMMA bars.

3.3 Evaluation of Poisson's ratio from DIC

Averaged Poisson's ratio of the specimen's core was calculated using DIC results for both types of the bars. Poisson's ratio was calculated using longitudinal and transverse displacements averaged per row or column, respectively. The ratio was calculated using the following formula (see Fig. 6):

$$\nu_{in3} = -\frac{L_{i4}\,(v_{11} - v_{12})}{H_{i1}\,(u_{41} - u_{42})} \tag{6}$$

Results of the Poisson's ratio calculated for both types of the experiments are shown in Fig. 9. The graph shows auxetic behavior of the lattice structure. The curves are in good agreement while results for the aluminium bars express slightly lower auxetic behavior that can be caused by influences summarized in section 3.1.

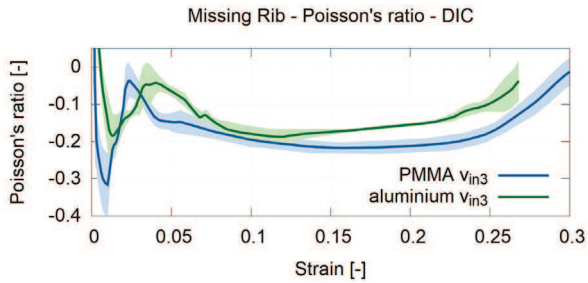

Fig. 9. Mean Poisson's ratio calculated from the experiments with aluminium and PMMA bars.

3.4 Stress-strain curves using DIC

Stress-strain curves with strain derived using DIC were calculated for both aluminium and PMMA bars. Stress-strain graphs using strains ϵ_{xx_e} (specimen edges) and $\epsilon_{xx_{in3}}$ (specimen's core) for both bar types are shown in Fig. 11 and Fig. 12. In case of the aluminium bars (Fig. 11), stress-strain curve corresponding to the specimen edges is almost identical with the strain-gauge curve (dashed line). Stress-strain curve corresponding to the specimen's core exhibits similar trends with the prolonged plateau region. In case of the PMMA bars (Fig. 12), the curve corresponding to the specimen edges is in very good agreement with the strain-gauge. Differences in the initial parts of the DIC curves to the strain-gauge curve are caused by low stiffness of the PMMA and the ramp-in effect of the shock wave in the specimen.

3.5 Full-field results

Full-field results were also calculated using DIC. Using 3×3 correlation sub-matrix for each correlation point, it was possible to calculate both longitudinal and transverse strains for every point in the correlation grid. Strains were then used for the calculation of Poisson's ratio in every correlation point using the standard formula $\nu = -\frac{\epsilon_{yy}}{\epsilon_{xx}}$. Example of full-field results is shown in Fig. 10. Results of full-field longitudinal strain are in very good agreement with other methods introduced in this paper. Localized strain-fields on the both sides of the specimen can be observed in the nominal strain as low as $\epsilon_{xx_e} = 0.05$ indicating that experiment was carried out in dynamic equilibrium. In the nominal strain approximately $\epsilon_{xx_e} = 0.18$ the deformation is distributed almost homogeneously through the specimen. Results of full-field Poisson's ratio exhibit very profound auxetic behavior with ratio reaching approx. -0.3 in the specimen's core. Auxetic behavior can be observed up to the nominal strain approx. $\epsilon_{xx_e} = 0.18$ where the structure stops to exhibit auxetic behavior.

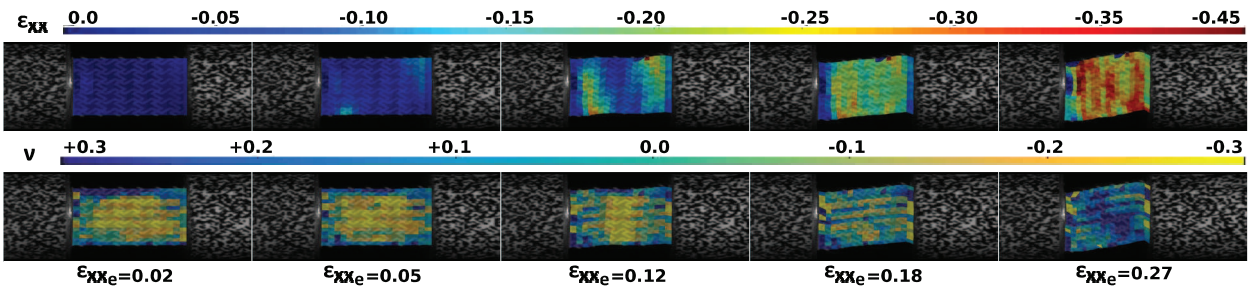

Fig. 10. Full-field analysis: in-plane longitudinal strain (first row), in-plane Poisson's ratio (second row).

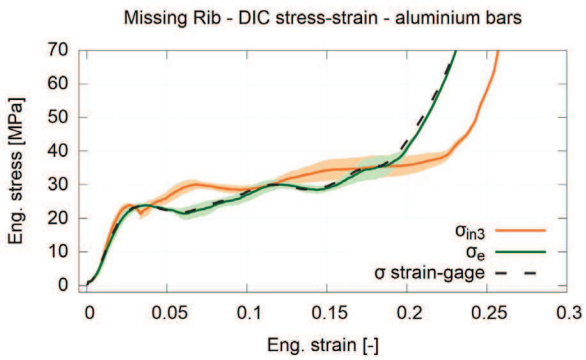

Fig. 11. DIC stress-strain curves for the boundary part of the specimen and for the specimen's core compared with the reference strain-gauge signal - aluminium bars.

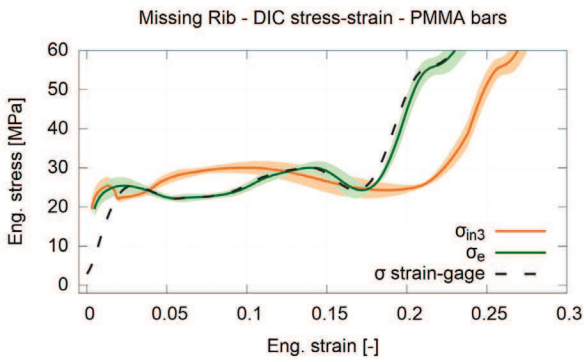

Fig. 12. DIC stress-strain curves for the boundary part of the specimen and for the specimen's core compared with the reference strain-gauge signal - PMMA bars.

4 Conclusion

Additively manufactured cut missing-rib auxetic lattice with 6×6 cells was subjected to dynamic compression using SHPB at strain rates $1500 - 2000\,\mathrm{s}^{-1}$. High-strength aluminium and PMMA bars were used in the experiments. SHPB stress-strain curves were compared with quasi-static data and significant strain-rate effect in the specimen was identified increasing the dynamic stresses by the factor of 1.4. Results derived from the aluminium and the PMMA bars are in very good agreement although the PMMA experiments were conducted at non-constant strain-rate and the specimen impedance was on the limit of PMMA causing significant non-linear effects that had to be corrected. All experiments were observed using the high-speed camera and the images were processed using DIC. DIC allowed for analysis of mean strain values in the different parts of the specimen showing different deformation behavior in the specimen's core during the experiment. Poisson's ratio was calculated using DIC in the selected region and was found to be negative. The aluminium bars indicated slightly lower ratio (approx. -0.15) than the PMMA bars (approx. -0.2). Full-field analysis was used for the evaluation of in-plane displacements and strains. The results were found to be in very good agreement with other methods and showed significant auxetic behavior of the specimen's core up to strain approx. 0.2 with Poisson's ratio reaching as low as approx. -0.3. To conclude, DIC and SHPB was successfully used as a tools for an advanced characterization of the additively manufactured auxetic lattice in dynamic compression.

The research was supported by the Czech Science Foundation (project no. 15-15480S) and the internal grant of the Czech Technical University in Prague (project no. SGS17/148/OHK2/2T/16).

References

1. Jung A., Diebels S., Mater. Des. **131**, 252-264 (2017)
2. Li T. et al., Mater. Des. **142**, 247-258 (2018)
3. Koudelka P. et al., Mater. Technol. **50**,311-317 (2016)
4. Xing H.Z. et al., Int. J. Impact Eng. **113**, 61-72 (2018)
5. Liu J. et al., Polym. Test. **36**, 101-109 (2014)
6. Islam M. A. et al., Int. J. Impact Eng. **114**, 111-122 (2018)
7. Gao G. et al., Eng. Fract. Mech. **138**, 146-155 (2015)
8. Bacon C., Exp. Mech. **38**, 242–249 (1999)
9. Zhao H., Gary G., J. Mech. Phys. Solids **45**, 1185-1202 (1997)
10. Jandejsek I. et al., In: *EAN 2010 Proceedings*, 121-126 (2010)
11. Lucas B. D., Kanade T., In: *Proceedings of Imaging Understanding Workshop*, 121-130 (1981)
12. Fíla T. et al., Adv. Eng. Mater. **19**, art. no. 1700076 (2017)